ELSEVIER

Contents lists available at ScienceDirect

# Optics and Laser Technology

journal homepage: www.elsevier.com/locate/optlastec





# Microlens arrays enable variable-focus imaging

Minjing Li<sup>a</sup>, Qing Yang<sup>a,\*</sup>, Hao Bian<sup>b</sup>, Tongzhen Yang<sup>a</sup>, Xun Hou<sup>b</sup>, Feng Chen<sup>b,\*</sup>

- <sup>a</sup> School of Mechanical Engineering, Xi'an Jiaotong University, Xi'an 710049, PR China
- b State Key Laboratory for Manufacturing System Engineering and Shaanxi Key Laboratory of Photonics Technology for Information, School of Electronic Science and Engineering, Xi'an Jiaotong University, Xi'an 710049, PR China

#### ARTICLE INFO

Keywords:
Microlens array
Multi-focus imaging
Femtosecond laser processing
Micro optics

#### ABSTRACT

Microlens array (MLA) is a key part of optical element for biomedical inspection, lab-on-a-chip device, and light-field cameras. However, conventional MLAs always have only one focal plane, which makes them difficult to capture targets at different positions. To solve this problem, a planar multi-focus MLA (MF-MLA) was prepared on a polydimethylsiloxane (PDMS) substrate by a combination of femtosecond laser wet etching (FLWE) and soft lithography techniques. The modulation transfer function (MTF) values of the microlenses all exceeded 0.2 when the spatial frequency was less than 200 lp/mm, indicating the high imaging ability of the lenses. The reported MF-MLA had three different focal lengths, so that targets at different positions could be easily imaged on a single image sensor. In addition, MLAs with more focal points could be fabricated by selecting appropriate processing parameters. It is anticipated that the as-fabricated MF-MLA will become a promising device to improve the performance of the optical system, especially in optical remote sensing, biomedical imaging, and machine vision.

# 1. Introduction

Microlens array (MLA) has received increasing attention because of its wide applications in microfluidic system [1,2], light field regulation [3], three-dimensional (3D) display [4–6], and light extraction technique [7–9] and so on. With the increasing demands for miniaturization, intelligence, and integration, many researchers are putting a great deal of efforts to study MLA and pursuing higher optical performance. Various processing methods have been proposed [10–17] for fabricating MLA. For example, Kirner's group reported a large-area MLAs on a fused silica by photoresist thermal-reflow and subsequent reactive ion etching [18]. Xu et al. prepared a plano-convex MLA based on a selective wetting surface [19]. The substrate was first modified with a hydrophobic film with patterned hydrophilic microhole array. The liquid photocurable polymer on the substrate flowed to the hydrophilic area and then formed a droplet array on the substrate due to the surface tension. The droplet arrays were finally curved by ultraviolet irradiation. Zhang et al. achieved an infrared MLA by a combination of an ultra-precision diamond milling and glass molding technique [20]. However, these methods are easy to fabricate microlenses with same curvatures on one surface, which unable to meet some practical requirements. For instance, in the 3D microscopic imaging of biomedical samples, only the objects at the focal plane can be clearly seen while other parts are blurry. In order to

get a holonomic image, a system with multi-lens optics is required, which makes it complex and bulk. Although the curved artificial compound eyes (ACEs) can provide a solution for solving this problem, their preparation still has some obstacles. Moreover, almost all current commercial photodector arrays are flat because of the processing technology [21] while the focal plane of the curved ACEs is non-planar. It is necessary to add an optical relay to associate the ACEs with plane sensors, such as optical fibers and lens group [22–26]. Recently, flat multifocus MLAs (MF-MLAs) have been fabricated by femtosecond laser-induced two-photon polymerization, multilayer photolithography and inkjet printing on circular confinement platforms [13,27–29]. Some of the methods suffer from a complex fabrication process, high cost or fabricated microlenses with poor optical imaging performance. Thus, a method to prepare flat MF-MLA with excellent optical properties at high efficiency and low cost is highly desired.

Recently, femtosecond laser has been proved to be an important tool for micro/nano processing because of its high flexibility and controllability [30–37]. Using femtosecond laser modification and subsequent chemical polishing can greatly improve the processing efficiency and microlens surface quality. Deng *et al.* prepared a compound infrared microlens array with ultrashort focal length by deposit a gradient-index lens on the convex polydimethylsioxane (PDMS) lens surface [38]. The convex microlenses was fabricated by soft lithography using a concave

E-mail addresses: yangqing@mail.xjtu.edu.cn (Q. Yang), chenfeng@mail.xjtu.edu.cn (F. Chen).

<sup>\*</sup> Corresponding authors.

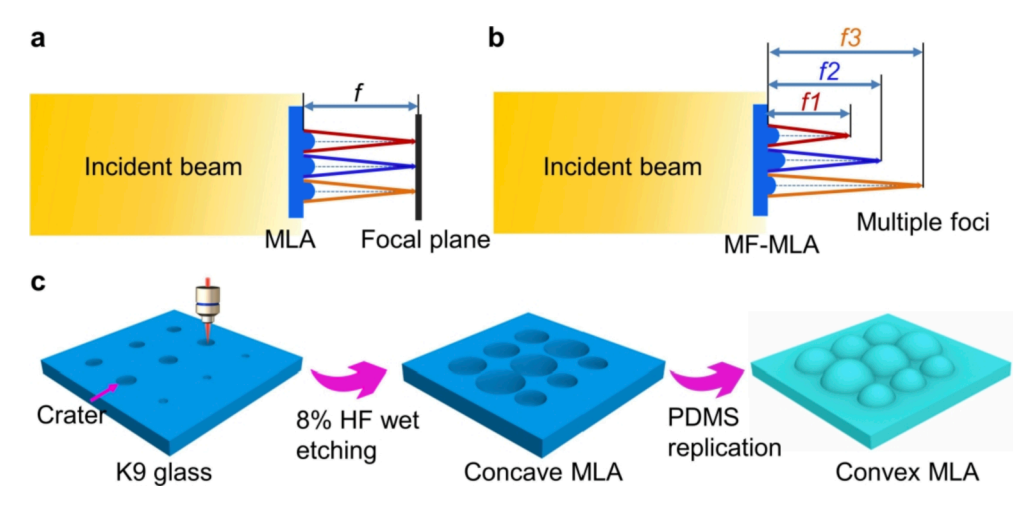


Fig. 1. (a) Focus principle of a conventional MLA. (b) Focus principle of the MF-MLA. (c) Schematic illustration of the fabrication process of MF-MLA.

MLA template prepared by femtosecond laser-assisted wet etching on a fused silica substrate. The as-prepared device has excellent imaging performance. Although the above method has been introduced for the fabrication of MLA, integrating the microlenses with different focal lengths on a lens array using this method is rarely investigated.

In this paper, microlenses with different focal lengths were fabricated on one lens array via femtosecond laser wet etching (FLWE) and soft lithography technique. The variation of different processing parameters (such as laser pulse energy, laser pulse number, and laser focusing position) on the geometry and focal lengths of the microlenses was systematically investigated. The significant curvature changes of the lenses can be obtained by accurately adjusting the focus position of laser beam on the sample along the beam propagation direction. The optical performance of the microlenses was quantified by measuring the optical modulation transfer function (MTF). As a representative example, we show the optical performance of a MF-MLA with three different focal planes. Each unit in the MF-MLA possesses a different focal length and also exhibits high image and focusing abilities. In addition, MLA with more focal planes could also be prepared by choosing suitable processing parameters.

#### 2. Results and discussion

### 2.1. Design and fabrication of the MF-MLA

Fig. 1a, b depicts the schematic diagram of working principle of two kinds of MLAs. For a conventional MLA, each lenslet in the array has the same focal length, which can only capture the target at a fixed position (Fig. 1a). On the contrary, microlenses in the MF-MLA have different focal lengths, which can be used for variable-focus imaging (Fig. 1b). In addition, the focal planes are controllable by changing the curvatures of the unit lenses. K9 glass (Union Optic, China) was used in this experiment and it was fixed on a 3D translation platform (H101A ProScan II Upright). The laser pulses (a repetition frequency of 1 kHz and pulse duration of 50 fs.) was generated from a Ti:sapphire laser system (Coherent Libra-usp-he) that operated at a wavelength of 800 nm. The fabrication of MF-MLA can be divided into three steps: femtosecond laser induced different modified craters, HF wet etching and PDMS replication. As shown in Fig. 1c, the laser beam was focused on the sample surface using an objective lens ( $50 \times$ , NA = 0.80, Nikon, Japan) to form laser-modified craters that were prepared under different processing parameters. The formation mechanism of the ablation crater is as follows: Laser beam is absorbed into the substrate through nonlinear effect such as multiphoton ionization and avalanche. With the rapid increase of electron concentration, Coulomb explosion, phase explosion and other damage processes are produced, thus forming a conical crater

on the surface, as shown in Fig. S1a in Supplementary Material. The shock waves from the explosion not only cause permanent damage to the material, but also form periodic nanostripes around the crater. At the same time, the high pressure shock waves compress the crystal lattice of the material, forming a Lewis base that is more likely to react with hydrofluoric (HF) acid [39,40]. The pulse energy was adjusted via an attenuator, and the number of pulses and laser focusing position were changed through computer program. Then, the substrate with laserinduced craters was etched down and polished by immersing into a HF solution with a volume fraction of 8% under an ultrasonic water bath. Laser-modified conical crater provides a channel for acid to enter into the material and the periodic nanostripes greatly increase the contact area between the solution and the substrate. In addition, the Lewis base further increases the reaction rate. Therefore, the etching rate of the modified area is much larger than that of the unirradiated area. As shown in Figure S1, the entire etching process can be divided into three stages: first, the nanostripes around the crater will be rapidly etched away under the influence of Lewis base (Fig. S1b, c); then the etching solution continues to polish the formed concave structure (Fig. S1d), and finally a concave microlens with a fine circular-shape is formed (Fig. S1e). Because the modified craters were fabricated under diverse parameters, the concave microlenses in the array had variable morphologies. At last, PDMS (Dow Corning 184) with a refractive index of 1.41, density of 1 g/mL, and transmission of 100 % was selected to replicate the concave MLA. In this experiment, the liquid PDMS mixture was solidified in an oven at 80 °C for 3 h. After demoulding, the PDMS sheet was cleaned in alcohol and deionized water for 5 min, respectively.

# 2.2. Control of the focal lengths of the microlenses

The multi-focus MLA was prepared by integrating microlenses with different focal lengths in an array. Therefore, it's important to explore the influence of various parameters such as laser pulse energy, number of pluses, and laser focusing position on the focal lengths of the microlenses. In each set of parameters, we prepared at least five lenses and averaged their diameters and sag heights as their geometrical dimension. All the PDMS microlenses were replicated from the K9 glass molds. The diameter (*D*) and sag height (*h*) of each lenslet was tested by using a LEXT-OLS4000 laser confocal microscope (Olympus, Japan) and its focal length was calculated using the following equations [39]:

$$R = \frac{h^2 + r^2}{2h} \tag{1}$$

$$f = \frac{R}{n-1}$$
 (2)

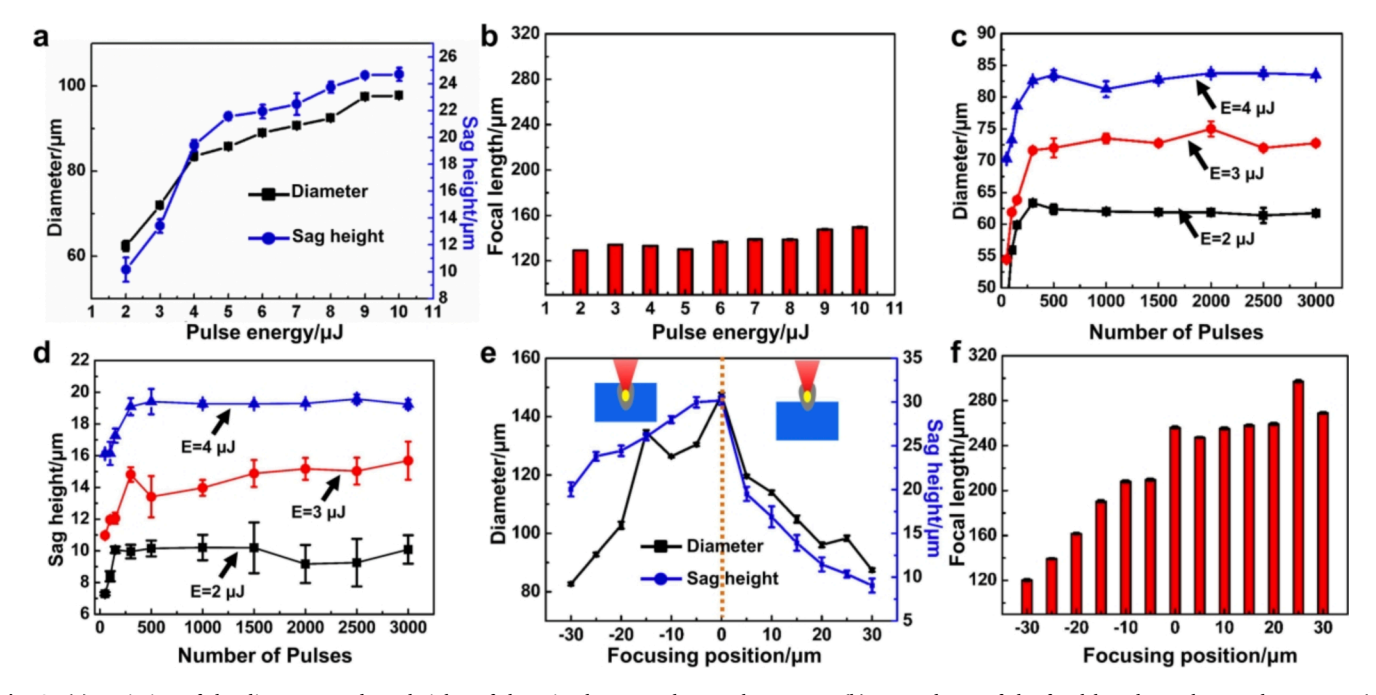


Fig. 2. (a) Variation of the diameters and sag heights of the microlenses on laser pulse energy. (b) Dependence of the focal lengths on laser pulse energy. (c) Relationship between the diameters and number of pulses at different laser pulse energy. (d) Relationship between the sag heights and number of pulses at different laser pulse energy. (e) Effects of the focusing position on the diameters and sag heights of the microlenses. (f) Effects of the focusing position on the focal lengths of the microlenses.

where R is the curvature of the microlens, r(r=D/2) refers the radius of the microlens, n is the refractive index of the PDMS (n=1.41), f is the focal length.

Laser pulse energy directly affects the area of the modified region, which in turn determines the final size of the microlenses after etching. In this case, each crater was ablated by 500 pulses and etched for 50 min. As shown in Fig. 2a, the size of the microlens is positively correlated with the laser pulse energy. As the pulse energy increases from 2 µJ to 5 μJ, the diameters and heights of the microlenses both increases rapidly, then go into a slow increase (6  $\mu$ J < E < 8  $\mu$ J), and finally remain stable  $(E > 9 \mu J)$ . As the pulse energy increases, the area of the modified region also increases, but eventually tends to a stable value, resulting in a corresponding change in size. The focal lengths of the microlenses are calculated to be 129.22, 134.21, 133.19, 130.2, 136.83, 138.95, 138.83, 147.71, and 149.55 μm, respectively. To quantitatively show the relationship, the graph of the focal lengths and pulse energy is plotted (Fig. 2b). It can be easily obtained that all the values in the range of 120  $\mu m - 140 \mu m$ , such close values are not optimal for the preparation of MF-MLAs.

Subsequently, the influence of pulse number on the lens size was also investigated. The laser pulse energy was set to 2  $\mu$ J, 3  $\mu$ J, and 4  $\mu$ J, and the number of pulses was set to 50, 100, 150, 300, 500, 1000, 1500, 2000, 2500, and 3000. As shown in Fig. 2c, d, when the number of laser pulses is less than 500, the size of the microlens changes with the increase of pulse number, and when it is more than 500 pluses, their size keep almost the same (the average diameters and sag heights of the microlenses are 62  $\mu m$  and 10  $\mu m$  for  $E=2~\mu J, 73~\mu m$  and 15  $\mu m$  for E= $3~\mu J,$  and  $83~\mu m$  and  $19~\mu m$  for  $E=4~\mu J). In addition, the regularity$ remains consistent when the pulse energy is different. This is due to the fact that when the number of laser pulses is small, the area of laser modified area is small. As the laser pulses increases, the energy deposited in the laser irradiated area gradually spreads, resulting in an increase of material modified area. Nevertheless, when the number of laser pulses exceeds 500, the area of the ablation crater obtained is large enough that the subsequent focused pulse energy is incapable of directly interacting with the surface and thus does not cause further damage to

the material surface.

Additionally, laser focusing position also has a great influence on the size of the ablation crater, which further affects the size of microlens. In this part, pulse energy was set as 5 µJ, each crater was ablated by 500 pulses and the sample was etched by 90 min. By adjusting the position of sample along the injected beam propagation direction, the laser pulses can focus at different position of the sample, such as  $-30 \mu m$ ,  $-25 \mu m$ , -20 μm, -15 μm, -10 μm, -5 μm, 0 μm, +5 μm, +10 μm, +15 μm, +20 $\mu m,\, +25\,\mu m,\, +30\,\mu m.$  The position where the laser is focused exactly on the sample is defined as  $Z=0~\mu m,$  where "Z = -X  $\mu m$ " means that the laser focus is at X µm below the sample surface (the left inset in Fig. 2e) and " $Z = +X \mu m$ " indicates the focus is at X  $\mu m$  above the sample surface (the right inset in Fig. 2e). The dependence of the diameters and sag heights of the microlenses on the laser focusing position is shown in Fig. 2e. The size of the microlenses decreases as the focal point moves away from the sample surface (The  $\emph{d}$  and  $\emph{h}$  are 82.69 and 20.02  $\mu m$ , 92.78 and 23.8  $\mu$ m, 102.8 and 24.44  $\mu$ m, 134.57 and 26.02  $\mu$ m, 126.39 and 28  $\mu m$ , 130.45 and 29.97  $\mu m$ , 147.39 and 30.19  $\mu m$ , 119.58 and  $19.51 \mu m$ , 114.02 and  $16.89 \mu m$ , 104.91 and  $13.92 \mu m$ , 96.07 and 11.47 $\mu m$ , 98.34 and 10.36  $\mu m$ , and 87.47 and 9.04  $\mu m$  respectively for focusing position equals to -30, -25, -20, -15, -10, -5, 0, +5, +10, +15, +20, +25, +30  $\mu m$ ). That's because the laser divergence becomes more serious as the focal point moves away from the surface, leading to a rapid decrease in the energy density of the laser spot. As a result, only a small area at the center of the spot is able to reach the damage threshold of the K9 glass, resulting in a rapid decrease of the size of the ablative crater and a decrease of the lens size. The focal lengths of the corresponding microlenses are shown in Fig. 2f. When the laser focusing position gradually moves from  $-30~\mu m$  to  $+30~\mu m$  at  $5~\mu m$  intervals, the values of the f are 128.54, 139.29, 161.63, 243.96, 208.08, 209.66, 256.19, 247.24, 255.27, 258.03, 259.31, 297.22, and 269.06  $\mu m$ , respectively. Due to the apparent differences between the focal lengths, microlenses fabricated under this set of data were mainly analyzed and used to fabricate a MF-MLA.

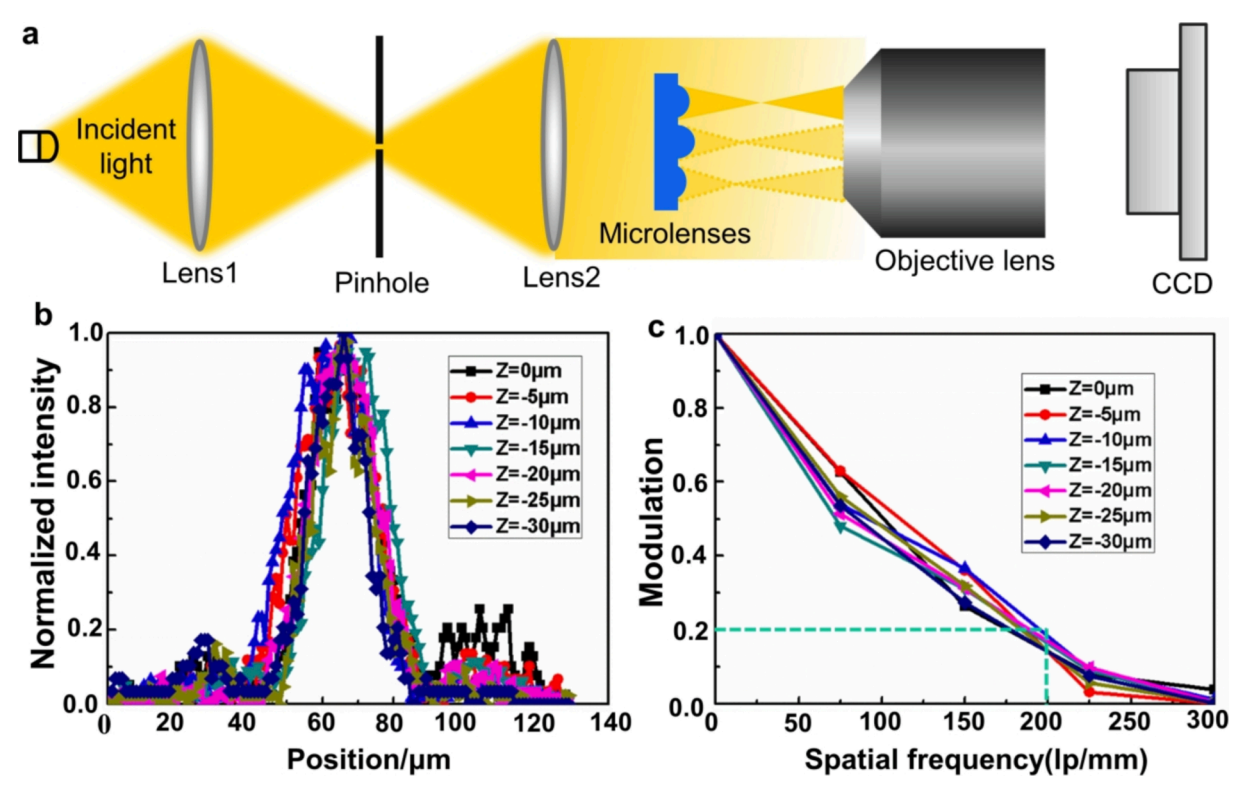


Fig. 3. (a) Schematic diagram of the PSF measuring system. (b) The measured PSFs of each microlens. (c) The calculated MTF of the microlenses.

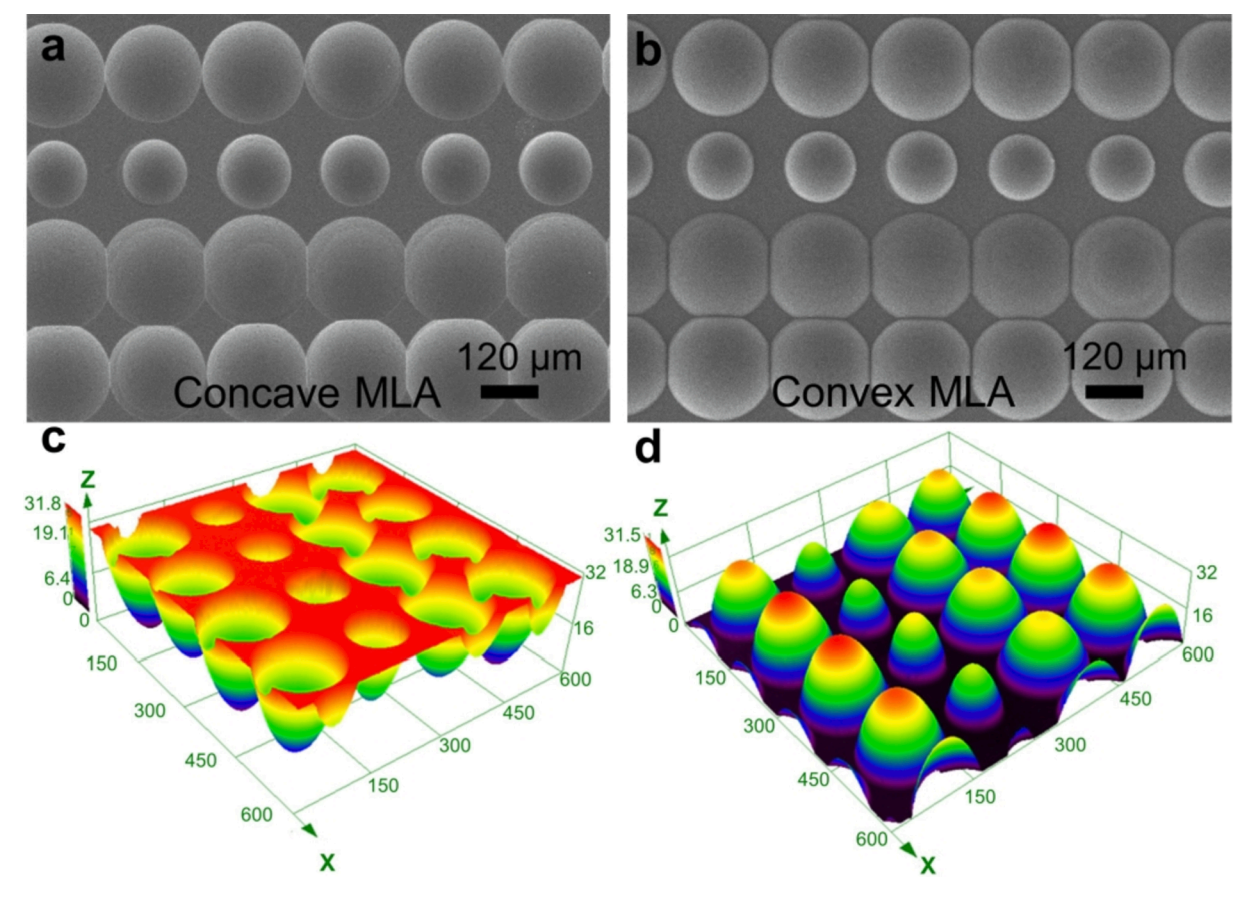


Fig. 4. SEM images of the MF-MLA before (a) and after (b) replication. (c) 3D morphology of the hard template. (d) 3D morphology of the multi-foci MLA respectively.

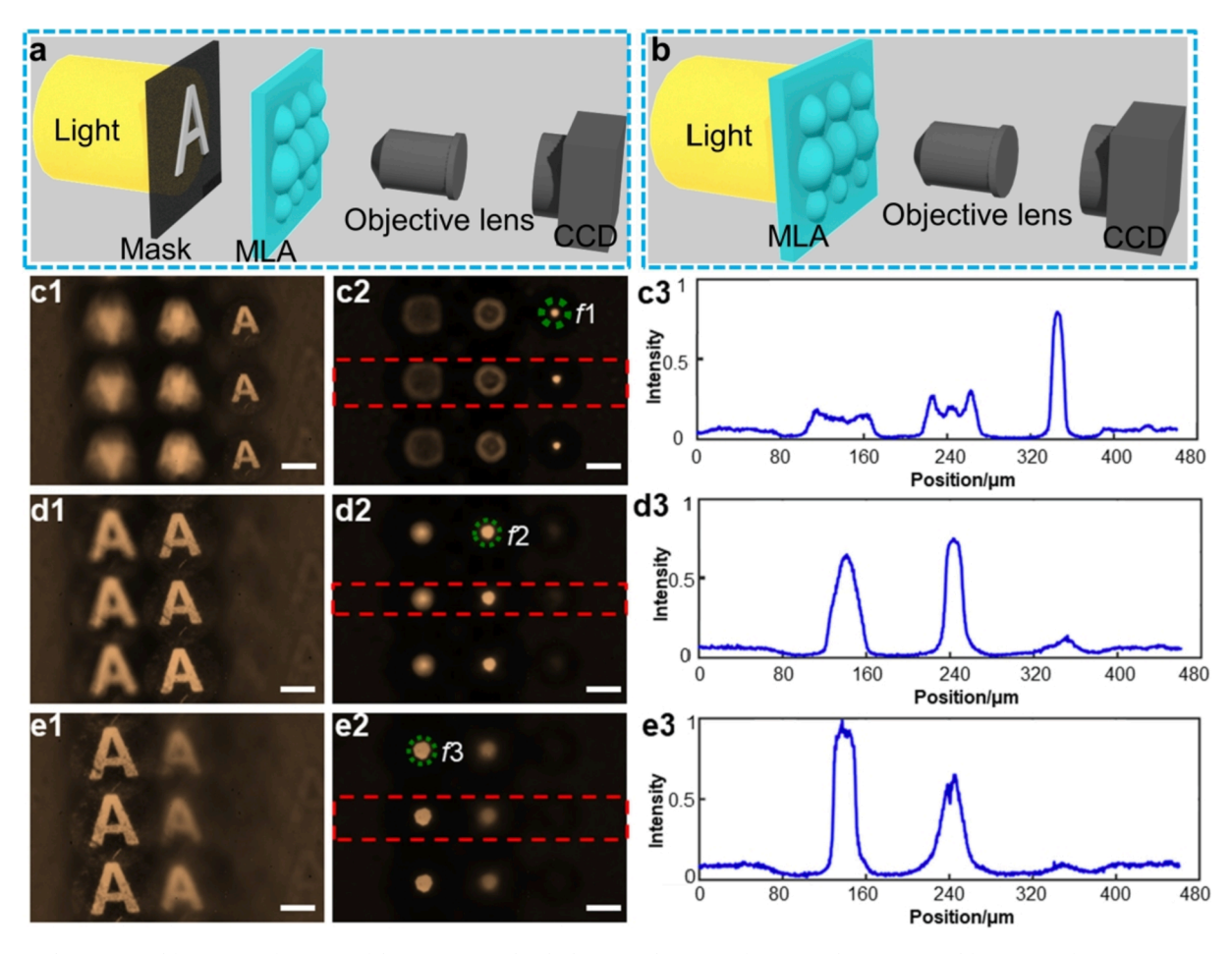


Fig. 5. Optical imaging and focusing performance of the MF-MLA. (a, b) The home-made systems for testing the imaging and focusing performance, respectively. (c1-e1) The imaging performance of the MLA at different positions: (c1) 128.54  $\mu$ m; (d1) 243.96  $\mu$ m; (e1) 256.19  $\mu$ m. (c2-e2) The focal images of microlens at the corresponding position. (c3-e3) Normalized intensity distribution of the focal spots (c2-e2). Scale bar is 50  $\mu$ m.

# 2.3. Quantitative analysis of imaging ability of the microlenses

MTF that is calculated from the point spread function (PSF) is one of the crucial parameters to evaluate the imaging ability of a microlens [41]. To quantitatively characterize the PSF of the prepared microlenes, a home-made system was set up, as shown in Fig. 3a. The incident light emitted by a tungsten lamp (Philip, LV-HL50W) passed through a pinhole (Thorlabs, P50D) and reached at a collimator lens. The microlenses were illuminated by the parallel beam and the foci were magnified by a  $50 \times$  objective lens (NA = 0.80), and then captured by a high sensitivity charge-coupled device (CCD) (Nikon, DS-Fi3). The normalized intensity of all measured 2D PSFs of the microlenses follows a Gaussian distribution, demonstrating the excellent focusing property (Fig. 3b). The MTF of each microlens was calculated by the Fourier transform of the corresponding PSF, as shown in Fig. 3c. It can be obtained that when the spatial frequency is less than 200 lp/mm, the MTF values of the microlenses prepared at different focusing position all exceed 0.2, indicating the great imaging ability of the lenses.

### 2.4. Morphology features of the hard template and MF-MLA

Because all lenses have excellent imaging ability and individual focal lengths, microlenses fabricated at Z = 0, Z =  $-15~\mu m$ , Z =  $-30~\mu m$  are selected to prepare MF-MLA as an example. The morphology of the K9 glass mold with concave MLA was observed through a scanning electron microscope (SEM) (FlexSEM1000, HITACHI, Japan), as shown in Fig. 4a. The units in the array are in a quadrilateral arrangement and those in the same line have same diameters and heights. From the first

line to the forth line, the microlenses were prepared at a focusing positon of 0  $\mu m, -30 \ \mu m, -15 \ \mu m,$  and 0  $\mu m.$  To precisely test the geometric size of lenses located at different columns, 3D morphography was measured by using the laser confocal microscope, as shown in Fig. 4c. The diameter and height of the microlenses from left to right are 146.92  $\mu m$  and 29.86  $\mu m, 136.5 \ \mu m$  and 25.2  $\mu m, 83.76 \ \mu m$  and 20.68  $\mu m,$  and 145.92  $\mu m$  and 29.86  $\mu m,$  respectively. After the replication process, the concave structures were perfectly transferred to the PDMS substrate. Fig. 4b, d shows the 2D and 3D images of the replicated MF-MLA. It is obvious that the as-prepared device has good morphology, which is close to the hard template. The diameter and height of the first microlens are 146.4  $\mu m$  and 29.58  $\mu m$ , the second are 132.5  $\mu m$  and 26.29  $\mu m$ , the third are 82.78  $\mu m$  and 20.39  $\mu m$ , and the last one are 147.4  $\mu m$  and 30.26  $\mu m$ . Compared to the mold, the geometric deformation is less than 150.6

### 2.5. Optical properties of the MF-MLA

Compared to the conventional MLA, the most remarkable feature of the MF-MLA is its multiple focal planes, which allows it to capture the object at different positions. The optical system in Fig. 5a is used to test the optical imaging performance of the as-prepared MLA. The image target with a transparent letter "A" was placed and fixed under the MF-MLA, perpendicular to the tungsten lamp light source. The objective lens (OL) and CCD camera were placed on the other side of the MLA. By moving the working position of the MLA, clear images of letter "A" could be constantly detected, as shown in Fig. 5c1-e1. When the sample was close to the OL, only the lenses located at the right column can image

(Fig. 5c1). As the sample gradually moving away from the OL, the second and first column could image, respectively (Fig. 5d1-e1). The imaging performance shows the extended depth-of-field ability of the MF-MLA.

In addition, the particular focusing characteristics and normalized intensity distribution of the focus were tested. The setup is schematically shown in Fig. 5b. The image target was removed and the bright spots formed at the specific focal plane and then captured with the CCD. Focus images of microlenses with focal lengths of 128.54, 243.96, and 256.19 μm are obtained. As shown in Fig. 5c2-e2, the microlenses at different positions are gradually focused as the distance between the objective lens and the sample increased from 128.54  $\mu m$  to 259.19  $\mu m.$  The crosssectional intensity distribution of the corresponding focus marked in the red dotted box is shown in Fig. 5c3-e3. When the sample is placed at the focal plane of one microlens, the relative light intensity is sharp and the other two are weak. In this paper, MLAs with three focal lengths mentioned above is just an example, people can also fabricate MLAs with more focus to meet their demands. The imaging and focusing ability of the MLAs with four and five foci were tested and the results can be seen in Fig. S2,3 of Supplementary Material.

#### 3. Conclusions

In summary, a convex MF-MLA has been fabricated on a PDMS substrate by femtosecond laser wet etching and lithography technique. Compared to the ordinary MLA with only one focal plane, the microlenses in the novel microlens array have different focal lengths and each of them can image dependently, which endow the MF-MLA capture targets at different positions. The microlenses show high optical quality with spatial resolution up to 175 lp/mm for imaging applications. Because of the flexibility and controllability of the femtosecond laser, people can selectively process MLAs according to their practical requirements. The as-prepared MF-MLA will hold great promise in the fields of optical remote sensing, biomedical imaging, mechanical optical alignment, and machine vision.

#### CRediT authorship contribution statement

Minjing Li: Writing – original draft, Conceptualization, Methodology. Qing Yang: Resources, Writing – review & editing. Hao Bian: Methodology. Tongzhen Yang: Data curation. Xun Hou: Resources. Feng Chen: Resources, Writing – review & editing.

# **Declaration of Competing Interest**

The authors declare that they have no known competing financial interests or personal relationships that could have appeared to influence the work reported in this paper.

### Acknowledgements

This work is supported by the National Science Foundation of China under the Grant nos. 62175195, 61875158, the International Joint Research Laboratory for Micro/Nano Manufacturing and Measurement Technologies, the Fundamental Research Funds for the Central Universities.

#### Appendix A. Supplementary data

Supplementary data to this article can be found online at https://doi. org/10.1016/j.optlastec.2022.108260.

#### References

- G. Holzner, Y. Du, X. Cao, J. Choo, A. J. deMello, S. Stavrakis, An optofluidic system with integrated microlens arrays for parallel imaging flow cytometry, Lab Chip 18 (23) (2018) 3631–3637.
- [2] V. Vespini, S. Coppola, M. Todino, M. Paturzo, V. Bianco, S. Grilli, P. Ferraro, Forward electrohydrodynamic inkjet printing of optical microlenses on microfluidic devices, Lab Chip 16 (2) (2016) 326–333.
- [3] Y. Wei, Q. Yang, H. Bian, F. Chen, M. Li, Y. Dai, X. Hou, Fabrication of high integrated microlens arrays on a glass substrate for 3D micro-optical systems, Appl. Surf. Sci. 457 (2018) 1202–1207.
- [4] K.-I. Joo, M.-K. Park, H. Park, T.-H. Lee, K.-C. Kwon, Y.-T. Lim, M.-U. Erdenebat, H. Lee, G. Lee, N. Kim, H.-R. Kim, Light-Field Camera for Fast Switching of Time-Sequential Two-Dimensional and Three-Dimensional Image Capturing at Video Rate, IEEE T. Ind. Electron. 67 (8) (2020) 6975–6985.
- [5] H.M. Kim, M.S. Kim, G.J. Lee, Y.J. Yoo, Y.M. Song, Large area fabrication of engineered microlens array with low sag height for light-field imaging, Opt. Express 27 (4) (2019) 4435–4444.
- [6] Y. Zhang, Y. Fu, H. Wang, H. Li, S. Pan, Y. Du, High resolution integral imaging display by using a microstructure array, J. Opt. Technol. 86 (2) (2019) 100–104.
- [7] S.-R. Shin, H.B. Lee, W.-Y. Jin, K.-J. Ko, S. Park, S. Yoo, J.-W. Kang, Improving light extraction of flexible OLEDs using a mechanically robust Ag mesh/ITO composite electrode and microlens array, J. Mater. Chem. C 6 (20) (2018) 5444–5452.
- [8] D. Yuan, B. Liu, Z. Zhu, Y. Guo, C. Cheng, H. Chen, M. Gu, M. Xu, L. Chen, J. Liu, X. Ouyang, Directional Control and Enhancement of Light Output of Scintillators by Using Microlens Arrays, ACS Appl. Mater. Interfaces 12 (26) (2020) 29473–29480.
- [9] J.-G. Zhou, X.-C. Hua, Y.-K. Chen, Y.-Y. Ma, C.-C. Huang, Y.-D. Wang, M.-K. Fung, Nano-modified indium tin oxide incorporated with ideal microlens array for light extraction of OLED, J. Mater. Chem. C 7 (13) (2019) 3958–3964.
- [10] J. Qiu, M. Li, H. Ye, C. Yang, C. Shi, Fabrication of high fill factor cylindrical microlens array with isolated thermal reflow, Appl. Opt. 57 (25) (2018) 7296–7302
- [11] Y. Hu, X. Zhu, H. Li, L. Qian, J. Yang, H. Lan, Fabrication of large-area cylindrical microlens array based on electric-field-driven jet printing, Microsyst. Technol. 25 (12) (2019) 4495–4503.
- [12] L. Jacot-Descombes, V.J. Cadarso, A. Schleunitz, S. Grutzner, J.J. Klein, J. Brugger, H. Schift, G. Grutzner, Organic-inorganic-hybrid-polymer microlens arrays with tailored optical characteristics and multi-focal properties, Opt. Express 23 (19) (2015) 25365–25376.
- [13] L. Wang, Y. Luo, Z. Liu, X. Feng, B. Lu, Fabrication of microlens array with controllable high NA and tailored optical characteristics using confined ink-jetting, Appl. Surf. Sci. 442 (2018) 417–422.
- [14] Q. Xu, B. Dai, Y. Huang, H. Wang, Z. Yang, K. Wang, S. Zhuang, D. Zhang, Fabrication of polymer microlens array with controllable focal length by modifying surface wettability, Opt. Express 26 (4) (2018) 4172–4182.
- [15] D. Li, B. Wang, Z. Qiao, X. Jiang, Ultraprecision machining of microlens arrays with integrated on-machine surface metrology, Opt. Express 27 (1) (2019) 212–224.
- [16] K. Lee, W. Wagermaier, A. Masic, K.P. Kommareddy, M. Bennet, I. Manjubala, S. W. Lee, S.B. Park, H. Colfen, P. Fratzl, Self-assembly of amorphous calcium carbonate microlens arrays, Nat. Commun. 3 (1) (2012) 1–7.
- [17] L.L. Ma, S.B. Wu, W. Hu, C. Liu, P. Chen, H. Qian, Y. Wang, L. Chi, Y.Q. Lu, Self-Assembled Asymmetric Microlenses for Four-Dimensional Visual Imaging, ACS Nano 13 (12) (2019) 13709–13715.
- [18] R. Kirner, J. Beguelin, M. Eisner, W. Noell, T. Scharf, R. Voelkel, Improvements on the uniformity of large-area microlens arrays in Fused Silica, Opt. Express 27 (5) (2019) 6249–6258.
- [19] M. Xu, Z. Zhou, Z.i. Wang, H. Lu, Self-Assembled Microlens Array with Controllable Focal Length Formed on a Selective Wetting Surface, ACS Appl. Mater. Interfaces 12 (6) (2020) 7826–7832.
- [20] L. Zhang, N.J. Naples, W. Zhou, A.Y. Yi, Fabrication of infrared hexagonal microlens array by novel diamond turning method and precision glass molding, J. Micromech. Microeng. 29(6) (2019) 065004.
- [21] D. Dumas, M. Fendler, F. Berger, B. Cloix, C. Pornin, N. Baier, G. Druart, J. Primot, E. le Coarer, Infrared camera based on a curved retina, Opt. Lett. 37 (4) (2012) 653–655.
- [22] K.H. Jeong, J. Kim, L.P. Lee, Biologically inspired artificial compound eyes, Science 312 (5773) (2006) 557–561.
- [23] D. Keum, K.W. Jang, D.S. Jeon, C.S.H. Hwang, E.K. Buschbeck, M.H. Kim, K. H. Jeong, Xenos peckii vision inspires an ultrathin digital camera, Light Sci. Appl. 7 (1) (2018) 1–7.
- [24] L. Li, A.Y. Yi, Design and fabrication of a freeform prism array for 3D microscopy, JOSA A 27 (12) (2010) 2613–2620.
- [25] C. Shi, Y. Wang, C. Liu, T. Wang, H. Zhang, W. Liao, Z. Xu, W. Yu, SCECam: a spherical compound eye camera for fast location and recognition of objects at a large field of view, Opt. Express 25 (26) (2017) 32333.
- [26] Y. Wang, C. Shi, C. Liu, X. Yu, H. Xu, T. Wang, Y. Qiao, W. Yu, Fabrication and characterization of a polymeric curved compound eye, J. Micromech. Microeng. 29 (5) (2019) 055008.
- [27] S.I. Bae, K. Kim, S. Yang, K.W. Jang, K.H. Jeong, Multifocal microlens arrays using multilayer photolithography, Opt. Express 28 (7) (2020) 9082–9088.
- [28] J.H. Lee, S. Chang, M.S. Kim, Y.J. Kim, H.M. Kim, Y.M. Song, High-Identical Numerical Aperture, Multifocal Microlens Array through Single-Step Multi-Sized Hole Patterning Photolithography, Micromachines (Basel) 11(12) (2020) 1068.

- [29] Z.N. Tian, W.G. Yao, J.J. Xu, Y.H. Yu, Q.D. Chen, H.B. Sun, Focal varying microlens array, Opt. Lett. 40 (18) (2015) 4222–4225.
- [30] M. Li, Q. Yang, J. Yong, J. Liang, Y. Fang, H. Bian, X. Hou, F. Chen, Underwater superoleophobic and anti-oil microlens array prepared by combing femtosecond laser wet etching and direct writing techniques, Opt. Express 27 (24) (2019) 35903–35913.
- [31] Z. Lin, M. Hong, Femtosecond Laser Precision Engineering: From Micron, Submicron, to Nanoscale, Ultrafast Science 2021 (2021) 1–22.
- [32] A. Pan, B. Gao, T. Chen, J. Si, C. Li, F. Chen, X. Hou, Fabrication of concave spherical microlenses on silicon by femtosecond laser irradiation and mixed acid etching, Opt. Express 22 (12) (2014) 15245–15250.
- [33] J. Yong, Q. Yang, J. Huo, X. Hou, F. Chen, Underwater Gas Self-Transportation along Femtosecond Laser-Written Open Superhydrophobic Surface Microchannels (< 100 μm) for Bubble/Gas Manipulation, Int. J. Extrem. Manuf. 4 (1) (2020), 015002.
- [34] J. Yong, Q. Yang, X. Hou, F. Chen, Emerging Separation Applications of Surface Superwettability, Nanomaterials 12 (4) (2022) 688.

- [35] J. Yong, Q. Yang, C. Guo, F. Chen, X. Hou, A review of femtosecond laserstructured superhydrophobic or underwater superoleophobic porous surfaces/ materials for efficient oil/water separation, RSC Adv. 9 (22) (2019) 12470–12495.
- [36] J. Yong, F. Chen, Q. Yang, X. Hou, Femtosecond laser controlled wettability of solid surfaces, Soft Matter 11 (46) (2015) 8897–8906.
- [37] D. Zhang, F. Chen, G. Fang, Q. Yang, D. Xie, G. Qiao, W. Li, J. Si, X. Hou, Wetting characteristics on hierarchical structures patterned by a femtosecond laser, J. Micromech. Microeng. 20(7) (2010) 075029.
- [38] C. Deng, H. Kim, H. Ki, Fabrication of a compound infrared microlens array with ultrashort focal length using femtosecond laser-assisted wet etching and dual-beam pulsed laser deposition, Opt. Express 27 (20) (2019) 28679–28691.
- [39] B. Hao, H.W. Liu, F. Chen, Q. Yang, P.B. Qu, G.Q. Du, J.H. Si, X.H. Wang, X. Hou, Versatile route to gapless microlens arrays using laser-tunable wet-etched curved surfaces, Opt. Express 20 (12) (2012) 12939–12948.
- [40] S. Tong, H. Bian, Q. Yang, F. Chen, Z. Deng, J. Si, X. Hou, Large-scale high quality glass microlens arrays fabricated by laser enhanced wet etching, Opt. Express 22 (23) (2014) 29283–29291.
- [41] F. Liu, Q. Yang, F. Chen, F. Zhang, H. Bian, X. Hou, Low-cost high integration IR polymer microlens array, Opt. Lett. 44 (7) (2019) 1600–1602.